Received: 6 November 2019 | Revised: 7 January 2021 | Accepted: 8 January 2021

DOI: 10.1111/bph.15385

RESEARCH PAPER

Therapeutic efficacy of the novel selective RNA polymerase I inhibitor CX-5461 on pulmonary arterial hypertension and associated vascular remodelling

Xia Xu[1] | Hua Feng[2] | Chaochao Dai[1] | Weida Lu[1] | Jun Zhang[3] | Xiaosun Guo[4] | Qihui Yin[4] | Jianli Wang[5] | Xiaopei Cui[1] | Fan Jiang[1,4]

[1]Department of Geriatrics & Key Laboratory of Cardiovascular Proteomics of Shandong Province, Qilu Hospital, Cheeloo College of Medicine, Shandong University, Jinan, Shandong, China

[2]Department of gastroenterology, Shandong Provincial Hospital Affiliated to Shandong First Medical University, Jinan, Shandong Province, China

[3]Department of Cardiovascular Surgery, Qilu Hospital, Cheeloo College of Medicine, Shandong University, Jinan, Shandong Province, China

[4]Department of Physiology and Pathophysiology, School of Basic Medicine, Shandong University, Jinan, Shandong, China

[5]Department of Obstetrics and Gynecology, Qilu Hospital of Shandong University, Jinan, Shandong, China

Correspondence
Xiaopei Cui and Fan Jiang, Department of Geriatrics, Qilu Hospital of Shandong University, 104 Wen Hua Xi Road, Jinan, 250012 Shandong, China.
Email:fjiang@sdu.edu.cn

Funding information
Key Research and Development Program of Shandong Province, Grant/Award Numbers: 2018GSF118011, 2019GSF108052, 2019GSF108114; National Natural Science Foundation of China, Grant/Award Numbers: 81500627, 81770469; Natural Science Foundation of Shandong Province, Grant/Award Numbers: ZR2015HQ029, ZR2017BH047

Background and Purpose: CX-5461 is a novel selective RNA polymerase I (Pol I) inhibitor. Previously, we found that CX-5461 could inhibit pathological arterial remodelling caused by angioplasty and transplantation. In the present study, we explored the pharmacological effects of CX-5461 on experimental pulmonary arterial hypertension (PAH) and PAH-associated vascular remodelling.

Experimental Approach: PAH was induced in Sprague–Dawley rats by monocrotaline or Sugen/hypoxia.

Key Results: We demonstrated that CX-5461 was well tolerated for in vivo treatments. CX-5461 prevented the development of pulmonary arterial remodelling, perivascular inflammation, pulmonary hypertension, and improved survival. More importantly, CX-5461 partly reversed established pulmonary hypertension. In vitro, CX-5461 induced cell cycle arrest in human pulmonary arterial smooth muscle cells. The beneficial effects of CX-5461 in vivo and in vitro were associated with increased activation (phosphorylation) of p53.

Conclusion and Implications: Our results suggest that pharmacological inhibition of Pol I may be a novel therapeutic strategy to treat otherwise drug-resistant PAH.

KEYWORDS
CX-5461, p53, pulmonary arterial hypertension, pulmonary arterial smooth muscle, RNA polymerase I inhibitor, vascular remodelling

Abbreviations: ATM, ataxia-telangiectasia mutated; ATR, ATM- and Rad3-related; MCT, monocrotaline; PAH, pulmonary arterial hypertension; PASMCs, pulmonary arterial smooth muscle cells; PCNA, proliferating cell nuclear antigen; Pol I, RNA polymerase I; rDNA, ribosomal DNA; RVSP, right ventricular systolic pressure; Su/H, Sugen/hypoxia; α-SMA, α-smooth muscle actin; β-Gal, β-galactosidase.

Xia Xu and Hua Feng contributed equally.

1 | INTRODUCTION

Pulmonary arterial hypertension (PAH) is a devastating clinical condition characterized by an increase in pulmonary circulatory resistance. Prolonged PAH may cause ventricular hypertrophy and right heart failure, which is the most common cause of death in critical patients (Lee & Rubin, 2005). Major pathophysiological mechanisms of PAH include exaggerated vasoconstriction, vascular remodelling and thrombosis (Humbert et al., 2004; Thompson & Lawrie, 2017). In addition, inflammation also plays a crucial role in the pathogenesis of PAH, supported by the accumulation of perivascular inflammatory cells (macrophages, dendritic cells, and lymphocytes) in the lungs and elevated levels of circulating inflammatory cytokines and chemokines in PAH patients (Price et al., 2012). Currently, three classes of drugs have been approved for the treatment of PAH, including prostacyclin analogues, endothelin receptor antagonists, and cGMP/cAMP-elevating agents. Despite the advent of these pharmacological agents, however, the overall mortality in patients with PAH remains high (Frumkin, 2012). Hence, identification of new biological targets for treating PAH is imperative.

Remodelling of small pulmonary arteries has a pivotal role in the pathogenesis of PAH, but therapies directly targeting this process are currently unavailable (Thompson & Lawrie, 2017). Pulmonary arterial remodelling in PAH is characterized by excessive muscularization of the vessel wall, of which aberrant proliferation of pulmonary arterial smooth muscle cells (PASMCs) is the primary pathological mechanism (Shimoda & Laurie, 2013; Tuder et al., 2007). Many factors can trigger the proliferative responses in PASMCs during PAH, including hypoxia, oxidative stress, and endothelin-1 (Hoidal et al., 2003; Janakidevi et al., 1992; Preston et al., 2006). Evidence has also pointed to a pivotal role of conventional inflammatory mediators in the maintenance of PASMC proliferation (Amsellem et al., 2017; Hurst et al., 2017; Wynants et al., 2012; Zabini et al., 2015). In addition, the importance of PASMC proliferation in PAH is also underscored by the hyperproliferative phenotype of PASMCs lacking the bone morphogenetic protein receptor type 2 (BMPR2), whose genetic mutations are the cause of familial PAH (Morrell, 2006).

RNA polymerase I (Pol I)-dependent ribosomal DNA (rDNA) transcription is a rate-limiting step in ribosome biogenesis and protein synthesis (Bywater et al., 2013; White, 2005). Ribosomal DNA transcription is generally thought to be a "housekeeping" process in cells, but this paradigm is now changing because inhibition of Pol I shows promising therapeutic effects on cancerous diseases, as reported by several recent studies (Bywater et al., 2013; Cornelison et al., 2017; Lee et al., 2017). In eukaryotic cells, inhibiting rDNA transcription triggers a conserved cellular stress response known as nucleolar stress, which subsequently causes activation of the tumour suppressor p53 (Boulon et al., 2010; Yang et al., 2018). Mounting evidence from both animal and human studies (including some very recent ones) has demonstrated that the level of p53 protein is decreased in PAH lungs (Abid et al., 2014; Jacquin et al., 2015; Liu et al., 2019; Wakasugi et al., 2019). In particular, reduced p53 protein in PASMCs may be implicated in the aberrant proliferation of the cells found in PAH (Jones et al., 2020; Wang et al., 2019). Restoration of the normal p53 functions has been linked to therapeutic effects on PAH in animal models (Abid et al., 2014; Jones et al., 2020).

What is already known

- CX-5461 is a novel selective RNA polymerase I inhibitor, which suppresses injury-induced arterial remodelling.

What this study adds

- CX-5461 inhibits experimental PAH and associated vascular remodelling and pulmonary inflammation.

What is the clinical significance

- Pharmacological inhibition of polymerase I may provide a novel therapeutic strategy to treat drug-resistant PAH.

In one of our recent studies we observed that inhibiting Pol I with CX-5461, the first-in-class selective Pol I inhibitor (Drygin et al., 2011), produced potent cytostatic effects in proliferating vascular SMCs, and effectively suppressed the development of neointimal hyperplasia induced by balloon injury in rat carotid arteries (Ye et al., 2017). These beneficial effects of CX-5461 were not associated with non-specific cytotoxicity or induction of cell apoptosis but appeared to be mediated by activation of the ataxia-telangiectasia mutated (ATM)/ATM- and Rad3-related (ATR)-p53 axis and cell cycle arrest in vascular SMCs (Ye et al., 2017). In another study, we have demonstrated that CX-5461 mitigates transplantation-induced peri-vascular inflammation and neointimal remodelling, at least partly by repressing macrophage-mediated innate immunity reactions (Dai et al., 2018). Particularly, we have demonstrated that induction of p53 phosphorylation (activation) is a robust cellular response to CX-5461 treatment in vascular smooth muscle cells (Ye et al., 2017). Given that pulmonary arterial remodelling in PAH shares similar signalling mechanisms with the process of neointimal hyperplasia caused by mechanical injuries (Houssaini et al., 2013; Paddenberg et al., 2007), in the present study we set out to characterize the pharmacological effects of CX-5461 on experimental PAH. Notably, a recently finished Phase I clinical trial has shown that intravenous administration of CX-5461 is well tolerated in patients with advanced haematological malignancies (Khot et al., 2019), highlighting potential clinical values for therapies with this new drug.

2 | METHODS

2.1 | Animals

All animal care and experimental studies were approved by the Qilu Hospital Animal Ethics Committee. Animal studies are reported in

compliance with the ARRIVE guidelines (Percie du Sert et al., 2020) and with the recommendations made by the *British Journal of Pharmacology* (Lilley et al., 2020). Male Sprague–Dawley rats of SPF grade (8–10 weeks of age, weighing 200–250 g each) were purchased from Charles River Laboratories (Beijing, China) and maintained on a standard laboratory rodent diet and autoclaved tap water ad libitum. Rats were housed in standard open-top polycarbonate cages (floor area 1,530 cm^2, four rats per cage) with corn cob bedding and maintained in an air-conditioned environment (non-SPF) with 12-h light/dark cycles. Only male Sprague–Dawley rats were used in this study because these animals were well-established PAH model following monocrotaline (MCT) or Sugen/hypoxia (Su/H) treatment as reported previously (Farhat et al., 1993; Spiekerkoetter et al., 2013). However, the present study would not exclude the possibility that the pharmacological effects observed in male animals might not be observed in females; this possibility needs additional investigations.

2.2 | Study design

All in vivo treatment studies were designed to generate groups of equal size, using randomization and blinded analysis. The minimum sample size for PAH models and various drug treatment groups was pre-determined to be $n \geq 8$ (see Table S1), calculated using an online tool (at https://www.stat.ubc.ca/~rollin/stats/ssize/n2.html), with estimated values of 30% mean difference and 20% variance. Three independent study cohorts were included: MCT)-prevention, MCT-reversal, and Su/H-reversal. Additionally, we included a separate validation cohort, with an extended observation period for survival following the MCT-prevention protocol. The dosage of CX-5461 used in rats was derived from previously published studies in mice (Bywater et al., 2013), according to principles given in Guidance for Industry: Estimating the Maximum Safe Starting Dose in Initial Clinical Trials for Therapeutics in Adult Healthy Volunteers, US Food and Drug Administration, 2005. CX-5461 of 12.5 $mg \cdot kg^{-1}$ (low dose) or 25 $mg \cdot kg^{-1}$ (high dose) was administered via gavage. CX-5461 was dissolved in 25-mM NaH_2PO_4 solution (pH 6.0) as described (Bywater et al., 2012). The NaH_2PO_4 solution alone was administered as vehicle control in PAH models. Gavage was performed at 9 am every 72 h. Subjects lost before the experimental endpoint were excluded from further haemodynamic, pathological, or biochemical analyses. For MCT-prevention experiments, animals were randomly divided into four groups: normal control, MCT, MCT plus low-dose CX-5461, and MCT plus high-dose CX-5461. MCT was given by a bolus injection (50 $mg \cdot kg^{-1}$ s.c.). CX-5461 treatment was started 3 days after MCT injection and continued until day 28 or 56. For MCT-reversal experiments, animals were randomly divided into three groups: normal control, MCT, and MCT plus low-dose CX-5461. CX-5461 treatment was started 21 days after MCT injection and continued to day 42. The stock solution of MCT was prepared by dissolving the compound in 1 N HCl followed by neutralization with 0.5 N NaOH as described (Farhat et al., 1993). Normal saline was used as vehicle for further dilutions. For Su/H-reversal experiments, animals were randomly divided into three groups: normal control, Su/H, and Su/H plus low-dose CX-5461. PAH was induced by a single subcutaneous injection of Sugen (20 $mg \cdot kg^{-1}$, DMSO as vehicle), followed by 3 weeks of exposure to hypobaric hypoxia (FiO_2 = 10%, equivalent to an altitude of 5,800 m) as described earlier (Dean et al., 2016; Nickel et al., 2015; Oka et al., 2007). Then the animals were returned to the normoxic environment for 2 weeks. After the 5-week induction period, CX-5461 treatment was initiated and continued for additional 3 weeks.

2.3 | Monitoring drug adverse effects

In vivo experiments were carried out in accordance with the principles outlined in Guide for the Care and Use of Laboratory Animals (8th edition, National Research Council, 2011). Specifically, potential adverse effects were assessed by monitoring typical signs of distress, including anorexia, rapid or laboured respiration, periocular and nasal porphyrin discharge, abnormal appearance or posture, and immobility. Body weight was measured every 3 days.

2.4 | Measurement of haemodynamic parameters

To measure right ventricular systolic pressure (RVSP) in rats, general anaesthesia was induced with 3% isoflurane inhalation and maintained with 1.5% isoflurane, using an anaesthesia machine (model R500, RWD Life Science, Shenzhen, China) connected to a mechanical ventilator (model DW-3000C, Zhenghua Bio-Instrument, Huaibei, Anhui Province, China). Tracheotomy and endotracheal intubation were performed. The ventilator frequency was 60 times per minute, and the tidal volume was 2 ml per 100-g body weight. An open-chest RV catheterization procedure was carried out as described (Handoko et al., 2009; Happe et al., 2016; Xu et al., 2011). Briefly, a lateral thoracotomy was made and the whole heart exposed quickly. A heparin-containing catheter with a 22G needle was connected to a pressure transducer (model YP100E, Yilian Medical Instrument, Shanghai). The needle was advanced into the right ventricle, and stabilization time (normally less than 5 min) was allowed until stable RV pressure patterns were observed. The signal was recorded using a BL-420E biological data processing system (Techman Co. Ltd., Chengdu, Sichuan Province, China). The system was calibrated using a mercury manometer. Immediately after the procedure, animals were killed with an overdose of pentobarbital. All of the operations and haemodynamic measurements were performed by a single researcher to eliminate possible technical biases. Any possible systemic bias in the invasive measurements would be offset by standardization of the surgical and recording procedures for all experimental groups. The ratio of RV weight to the sum of weight of left ventricle plus interventricular septum was used as an index of RV hypertrophy. In separate experiments, conscious systemic BP was measured using tail-cuff method with an automated non-invasive BP detector system (model BP-300A, Techman).

2.5 | Tissue collection and histopathological analysis

After killing with an overdose of pentobarbital, the animal was perfused with cold saline at 100 mmHg via the left ventricle until tissues became pale. The hilum of right lung was ligated and the lung was removed for biochemical analyses. Then the animal was perfused and fixed with cold 4% paraformaldehyde at 100 mmHg for 5 min. The remaining lung tissues were harvested and further fixed in 4% paraformaldehyde overnight at 4°C. Serial paraffin sections of 4-μm thickness were cut from the upper one third of lung (between the apex and hilum). Sections were stained with haematoxylin and eosin (H&E). Three non-consecutive sections were analysed for each animal, and ten random 200X fields were analysed per section. Images were captured using a light microscope (AxioLab A1, Zeiss, Jena, Germany). Morphometric measurements were performed using Image-Pro Plus 5.0 software (RRID:SCR_007369) (Media Cybernetics, Bethesda, MD, USA). The total cross-sectional area of a vessel was defined as that enclosed by the media/adventitia border. The relative lumen area was defined as the percentage value of absolute lumen area over the total vessel area. The measurement of mean intimal-medial thickness was carried out as described (Dai et al., 2018). For each vessel, the thickness at positions of 2, 4, 6, 8, 10, and 12 of clock was taken, and the averaged value was used as the mean thickness. Sections were also stained for elastic laminae with Verhoeff–Van Gieson staining as used previously (Jones et al., 2005). Histopathological analysis was performed by an independent researcher in a blind manner.

2.6 | Immunohistochemistry and immunofluorescence

Immunohistochemistry was conducted as described earlier (Ye et al., 2017). The antibody-based procedures used in this study comply with the recommendations made by the *British Journal of Pharmacology*. Sections were heated in citrate buffer (pH 6.0) and endogenous peroxidases inactivated with 3% hydrogen peroxide. Sections were incubated with primary antibodies at 4°C overnight followed by corresponding biotin-conjugated secondary antibodies at 37°C for 60 min. Colour development was performed with Vectastain Elite ABC Kit (Vector Laboratories, Burlingame, CA, USA) and diaminobenzidine (DAB) substrate. Negative controls were performed by replacing the primary antibody with non-immune IgG. Images were taken using an AxioLab A1 microscope (Zeiss). Semi-quantitative analysis on immunoreactivity was performed by measuring the percent area with positive staining, using Image-J software (NIH, USA) (RRID:SCR_003070) running with Colour Segmentation Plugin (http://bigwww.epfl.ch/sage/soft/colorsegmentation/), which allowed automatic colour separation based on a K-Means clustering algorithm. For immunofluorescence, cells were cultured on Lab-Tek II chamber slides (Thermo Fisher, Waltham, MA, USA) and fixed in cold methanol. Alexa Fluor-594 or Alexa Fluor-488-conjugated secondary antibodies were used for labelling. Cells were counterstained with DAPI and photographed with a fluorescent microscope (model Eclipse Ni-U, Nikon, Japan).

2.7 | Real-time PCR

Total RNA was extracted from lung homogenates using Trizol reagent (Thermo). cDNA was synthesized from 1 μg of RNA using PrimeScript RT reagents from TaKaRa (Shiga, Japan). Real-time PCR was performed using SYBR Green Master Mix from TaKaRa. A StepOne System (Applied Biosystems, Carlsbad, CA, USA) was used for PCR amplification, and the $2^{-\Delta\Delta CT}$ method was used to assess the relative mRNA expression level. Primers used were as follows: 45S pre-rRNA, forward TGCGGAAGGATCATTAACGG, reverse AAGAGCGAGAAAA CGGAGGA; 18S mature rRNA, forward CGCGGTTCTATTTTGTTGGT, reverse AGTCGGCATCGTTTATGGTC. The primers for 45S pre-rRNA targeted the junction area spanning the end of 18S rRNA and the first internal transcribed spacer (refer to RefSeq NR_046239.1) (RRID:SCR_003496).

2.8 | Cell culture

Human PASMCs were obtained from Chi Scientific (#1-0008, Suzhou, China) and cultured in DMEM/F12 medium supplemented with 10% FBS. Cells of passages 5 to 9 were used. Before experimentation, PASMCs were pre-stimulated with **PDGF-BB** (20 $ng \cdot ml^{-1}$, from R&D Systems, Minneapolis, MN, USA) for 24 h. Cell viability was determined with a colorimetric assay using Enhanced Cell Counting Kit-8 (#C0042, Beyotime, Beijing, China).

2.9 | Flow cytometry

Cells were detached with trypsin, fixed with 70% ice cold ethanol for 2 h, and stained with 50 $\mu g \cdot ml^{-1}$ of propidium iodide plus 500 $U \cdot ml^{-1}$ of RNase at 37°C in the dark for 30 min using a kit from Abcam (#ab139418). Cells were filtered through a 70-μm mesh, and analysed with a FACSCalibur flow cytometer (BD Biosciences, Mountain View, CA, USA). Cell doublets were excluded by gating on the fluorescence Width versus Area plot. Data acquisition was executed using CellQuest Pro software and further analysed with FlowJo software (BD Biosciences) (RRID:SCR_008520).

2.10 | Western blot and ELISA

Western blotting was conducted with the experimental detail provided conforming with the *BJP* guidelines (Alexander et al., 2018). Total protein was extracted from lung homogenates in a lysis buffer containing 50 mM Tris, pH 7.5, 2 mM EDTA, 100 mM NaCl, 50 mM NaF, 1% Triton X-100, 1 mM Na_3VO_4, 40 mM β-glycerol phosphate, and the protease inhibitor cocktail (Roche, Mannheim, Germany).

Following SDS-PAGE electrophoresis, proteins were transferred to nitrocellulose membranes. The membrane was blocked with 5% nonfat milk, incubated with primary antibodies overnight at 4°C, and developed using Immobilon Western Chemiluminescent HRP Substrate from Merck Millipore (Darmstadt, Germany). Developed membranes were scanned with a ChemiDoc XRS+ molecular imaging system (Bio-Rad, Hercules, CA, USA). Band densitometry analysis was performed using Image-J. The concentration of IL-6 was determined with an ELISA kit from Sigma-Aldrich (#RAB0312).

2.11 | Detection of cell senescence and apoptosis

To detect cell senescence, tissue sections were stained with a β-galactosidase (β-Gal) Staining Kit (#G1580, from Solarbio, Beijing, China) following the manufacturer's instructions. To detect apoptosis, tissue sections were stained with a Colorimetric TUNEL Apoptosis Assay Kit (#C1098, from Beyotime, Shanghai, China).

2.12 | Data and statistical analysis

The data and statistical analysis complied with the recommendations of the *British Journal of Pharmacology* on experimental design and analysis in pharmacology (Curtis et al., 2018). Data are presented as mean ± SD. The declared group size and the data points in graphs represent independent values and not technical replicates. Data analysis was performed using Prism (Version 8.0) from GraphPad Software (San Diego, CA, USA) (RRID:SCR_002798), with Mann–Whitney test (for two-group comparisons), one-way ANOVA followed by Tukey's test (for multiple comparisons of data passed Anderson-Darling normality test and with no variance inhomogeneity), or non-parametric Kruskal–Wallis test followed by Dunn's test (for multiple comparisons of non-normally distributed data). Post hoc test was only performed when the ANOVA achieved significance ($P < .05$). Kaplan–Meier survival curves were analysed using Logrank test. Statistical significance was determined by a fixed P value of <0.05 (two-tailed) throughout the results. Statistical analysis was undertaken only for studies where each group size was at least $n = 5$. Data normalization was carried out for western blot and cell viability assays to reduce unwanted sources of variation; values undergone normalization were from the same blot/culture plate. PCR data were processed and normalized according to the standard $2^{-\Delta\Delta Ct}$ method (Livak & Schmittgen, 2001). Normalized data were expressed as fold mean of the controls without actual units. No outliers were excluded in data analysis and presentation.

2.13 | Materials

CX-5461 was from ApexBio Technology LLC (Houston, TX, USA). Monocrotaline (MCT, #C2401) and Sugen (SU 5416, #S8442) were purchased from Sigma-Aldrich (St Louis, MO, USA). Pifithrin-α was purchased from Selleck Chemicals (Houston, TX, USA). Primary antibodies used were as follows: phospho-UBF1 (S484) (#ab182583, 1:100 for immunohistochemistry), proliferating cell nuclear antigen (PCNA) (#ab18197, 1:500 for immunofluorescence, RRID:AB_444313), α-smooth muscle actin (α-SMA, #ab5694, 1:200 for immunohistochemistry, RRID:AB_2223021), CD68 (#ab125212, 1:500 for immunohistochemistry, RRID:AB_10975465), CD4 (#ab203034, 1:400 for immunohistochemistry), CD8 (#ab33786, 1:200 for immunohistochemistry, RRID:AB_726709), and CD31 (#ab182981, 1:1500 for immunohistochemistry) were from Abcam (Cambridge, UK). Antibodies for p53 (#2524, 1:1000 for western blot, RRID:AB_331743) and phospho-p53 (Ser15) (#9284, 1:1000 for western blot and 1:150 for immunohistochemistry, RRID:AB_331464) were from Cell Signaling (Beverley, MA, USA).

2.14 | Nomenclature of targets and ligands

Key protein targets and ligands in this article are hyperlinked to corresponding entries in http://www.guidetopharmacology.org and are permanently archived in the Concise Guide to PHARMACOLOGY 2019/20 (Alexander et al., 2019).

3 | RESULTS

3.1 | Tolerance to CX-5461 treatment

As compared to untreated PAH models, animals treated with either low-dose (12.5 $mg \cdot kg^{-1}$) or high-dose (25 $mg \cdot kg^{-1}$) CX-5461 did not show additional or exacerbated signs of distress (see Methods), except for some increased anorexia in subjects treated with high-dose CX-5461. These animals did not lose body weight during the treatment, although the rate of body weight gain was reduced (not statistically significant as compared to PAH models without treatment) (Table S1). Given that the overall survival was significantly increased by high-dose CX-5461, it was argued that the change in body weight gain did not represent a major adverse impact. Nevertheless, based on the effectiveness of low-dose CX-5461 in the prevention experiment and the principles of 3Rs (Sneddon et al., 2017), we excluded additional high-dose groups in the following reversal experiments. In the Su/H-reversal cohort, low-dose CX-5461 treatment significantly increased the body weight gain (Table S1).

3.2 | CX-5461 inhibits the development of MCT-induced PAH and pulmonary arterial remodelling

Treatment with CX-5461 at both low and high doses retarded similarly the development of MCT-induced PAH, as shown by the decreased RV pressure and RV hypertrophy (Table 1 and Figures S1 and S2). CX-5461 at the high dose had no significant effect on the systemic BP (Con 116.9 ± 10.8; MCT 107.0 ± 12.6; MCT + CX-5461 116.7 ± 4.5, systolic pressure in mmHg, mean ± SD, $n = 5$ each). Histological

TABLE 1 Effects of CX-5461 treatment in vivo on pulmonary haemodynamic parameters in different PAH models

	Treatment groups			
Study design	**Con**	**PAH**	**PAH + CXL**	**PAH + CXH**
Prevention cohort (MCT)				
RVSP (mmHg)	39.0 ± 3.5 (6)	75.6 ± 8.9# (6)	37.0 ± 13.2* (6)	54.4 ± 11.5* (6)
RV hypertrophy index	0.26 ± 0.04 (6)	0.56 ± 0.17# (6)	0.31 ± 0.04* (6)	0.33 ± 0.06* (6)
Reversal cohort (MCT)				
RVSP (mmHg)	36.5 ± 8.1 (6)	78.0 ± 9.8# (6)	52.7 ± 19.4* (6)	–
RV hypertrophy index	0.33 ± 0.11 (6)	0.63 ± 0.05# (6)	0.53 ± 0.11 (6)	–
Reversal cohort (Su/H)				
RVSP (mmHg)	40.7 ± 9.7 (6)	82.7 ± 20.0# (6)	58.7 ± 16.1* (6)	–
RV hypertrophy index	0.34 ± 0.12 (6)	0.68 ± 0.21# (6)	0.55 ± 0.09 (6)	–

All data are expressed as mean ± SD. The *n* numbers for each group were shown in brackets.
#$P < .05$, significantly different from Con;
*$P < .05$, significantly different from PAH; one-way ANOVA (for normally distributed data) or Kruskal–Wallis test (for non-normally distributed data).
Con, normal controls receiving no treatment; CXH, PAH animals treated with high-dose CX-5461 (25 mg·kg^{-1}); CXL, PAH animals treated with low-dose CX-5461 (12.5 mg·kg^{-1}), PAH, disease models serving as vehicle controls; RVSP, right ventricular systolic pressure.

examinations on small pulmonary arteries with external diameters between 20 to 100 μm revealed that PAH was associated with narrowing of the vessel lumen and muscularization of the vessel wall, as indicated by the increase in intimal-medial thickness (Shimoda & Laurie, 2013). CX-5461 ameliorated the narrowing of vessel lumen and significantly reduced the intimal-medial thickness (Figure 1a,b). To directly assess the effect of CX-5461 on muscularization, we stained the cross-sections with immunohistochemistry for the smooth muscle marker α-SMA, and quantified the occupancy (% of total cross-sectional area) of SMA-positive cells in the vessel wall. MCT significantly increased the level of muscularization, which was attenuated significantly by CX-5461 (Con 46.5 ± 1.6%; MCT 93.7 ± 3.8%; MCT + low-dose CX-5461 55.5 ± 7.6%, $n = 6$). Moreover, some arteries with vaso-occlusive lesions (obliterated vessels) (Shimoda & Laurie, 2013) were found in MCT-treated lungs (see Figure 1a). The occlusive lesion was positive for α-SMA, but almost negative for the endothelial cell marker CD31 (Figure 1c). CX-5461 treatment significantly reduced the number of obliterated vessels (Figure 1d). Verhoeff–Van Gieson staining indicated that MCT-induced vascular remodelling was primarily due to increased muscularization of the medial layer, whereas formation of neointima was minor.

Cell proliferation requires increased rates of ribosome biogenesis and thereby rDNA transcription (White, 2005). To clarify whether Pol I-dependent rDNA transcriptional activity was altered during PAH development, we measured the ratio of 45S pre-rRNA to 18S mature rRNA with quantitative PCR. This ratio was significantly increased in MCT-treated lungs but remained unchanged in CX-5461 co-treated lungs (Figure 2a). Then we examined the level of UBF phosphorylation as a measure of the global rDNA transcriptional activity and found that UBF phosphorylation was elevated in the tunica media of pulmonary arteries in MCT-treated lungs (Figure 2b). These findings indicated that PAH-associated arterial remodelling was accompanied by an increase in the rate of rDNA transcription. However, as a factor upstream of Pol I functions and rDNA transcription, UBF activation (phosphorylation) was very unlikely to be modulated by CX-5461.

3.3 | CX-5461 therapy reverses established PAH

Next we tested whether CX-5461 had any beneficial effects on pre-existing PAH. In the MCT-induced PAH model, low-dose CX-5461 at 21 days after MCT administration significantly reduced RV pressure (Table 1 and Figure S1). This effect was accompanied by amelioration of pulmonary vascular remodelling (Figure 3a). However, RV hypertrophy was not significantly changed by CX-5461 (Table 1 and Figure S1). Interestingly, we found that CX-5461 reversed the increased level of cellularity in MCT-treated lungs (Figure 3b). Most of the cellular clumps found in MCT-treated lungs exhibited a perivascular localization, which appeared to reflect the increased perivascular inflammation in PAH as reported by others (Savai et al., 2012). To further confirm the disease reversal activity of CX-5461 on established PAH, we tested the effects of low-dose CX-5461 in Su/H models. Similar to the findings in MCT-treated lungs, CX-5461 ameliorated the narrowing of vessel lumen and reduced the mean intimal-medial thickness (Figure 3c). The rate of vessel obliteration was also reduced by CX-5461 (Figure 3d). In contrast to MCT-induced vessel remodelling, the occlusive lesions induced by Su/H were primarily due to growth of the neointima (Figure 3e). Immunohistochemistry demonstrated that the neointimal tissues were mainly positive for CD31 (Figure 3e). Moreover, we showed that CX-5461 significantly reduced the elevated RV pressure in Su/H animals, whereas RV hypertrophy was not changed (Table 1 and Figure S1).

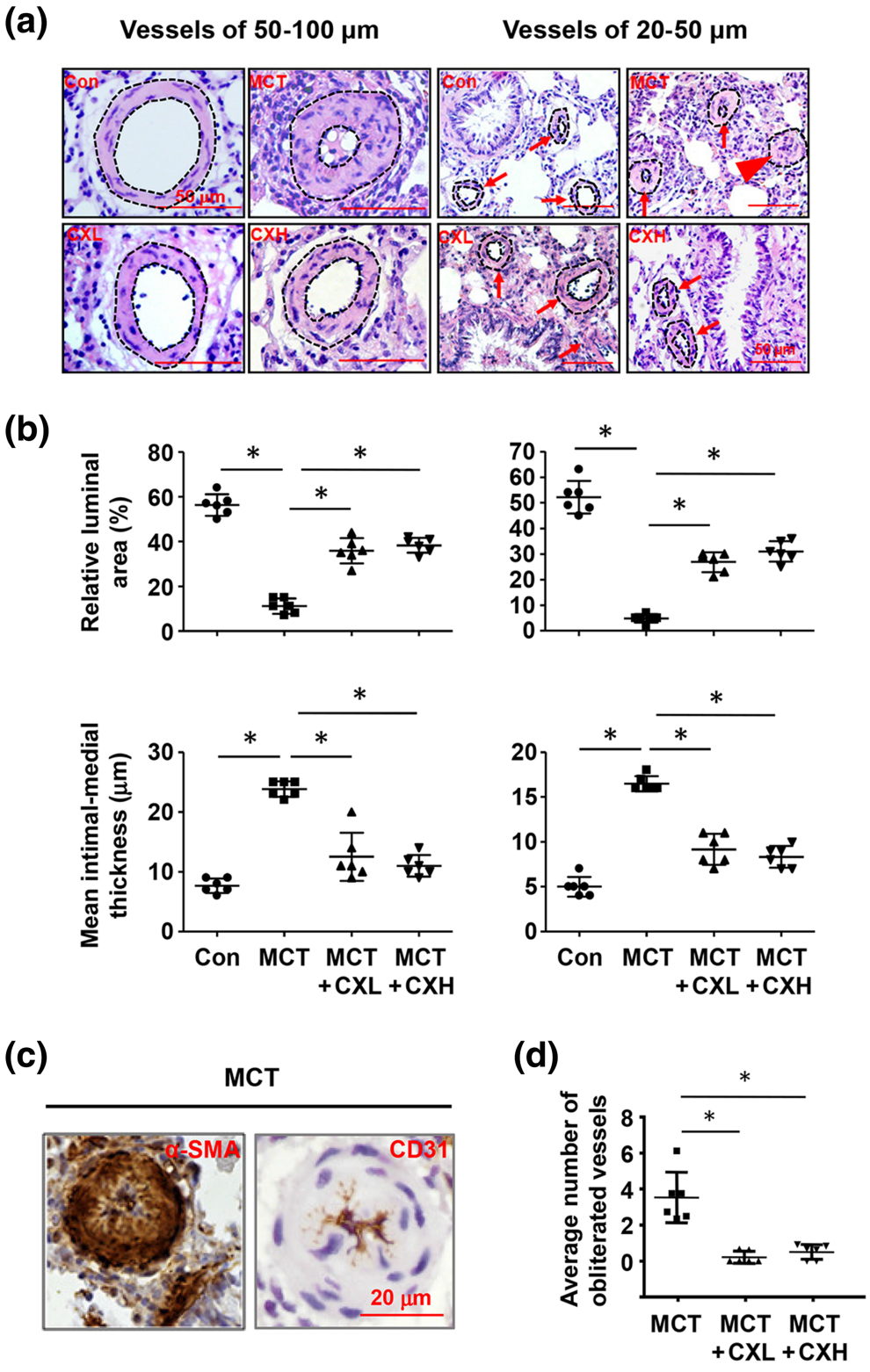

FIGURE 1 Effects of CX-5461 co-treatment on monocrotaline (MCT)-induced pulmonary arterial remodelling. (a) H&E-stained lung sections showing the effects of CX-5461 on vascular remodelling of pulmonary arteries of different calibre. Small arteries are indicated by arrows. A vessel with occlusive lesion is indicated by the arrowhead. Dashed lines denote the lumen/vessel wall border and media/adventitia border respectively. (b) Quantitative data showing changes in percent luminal area and mean intimal-medial thickness of pulmonary arteries with diameters of 50–100 μm (left panels) and 20–50 μm (right panels) respectively. (c) Immunohistochemical images showing that the occlusive lesion in MCT-treated lungs is positive for the smooth muscle marker α-SMA (brown colour, counterstained with haematoxylin), but almost negative for the endothelial cell marker CD31 (note the endothelium is positive for CD31 as shown by the brown colour). (d) Effects of CX-5461 on the rate of vessel obliteration in MCT-treated animals (average number per 200X field). Data are mean ± SD. *P < .05, significantly different as indicated; one-way ANOVA. Con, normal controls receiving no treatment; MCT, disease models serving as vehicle control; CXL/CXH, PAH animals treated with low-dose (12.5 mg·kg^{-1}) /high-dose (25 mg·kg^{-1}) CX-5461

3.4 | Effects of CX-5461 on survival

In the MCT-prevention cohort, the overall Logrank test P value was 0.044, and the Logrank test for trend P value was 0.0229 (Figure S3). Pairwise tests showed that the difference between MCT and high-dose CX-5461 groups was statistically significant, whereas the effect of low-dose CX-5461 did not reach significance. To further clarify the effectiveness of CX-5461 on survival, we employed a separate validation cohort with an extended observation period for 56 days following the MCT-prevention protocol. The

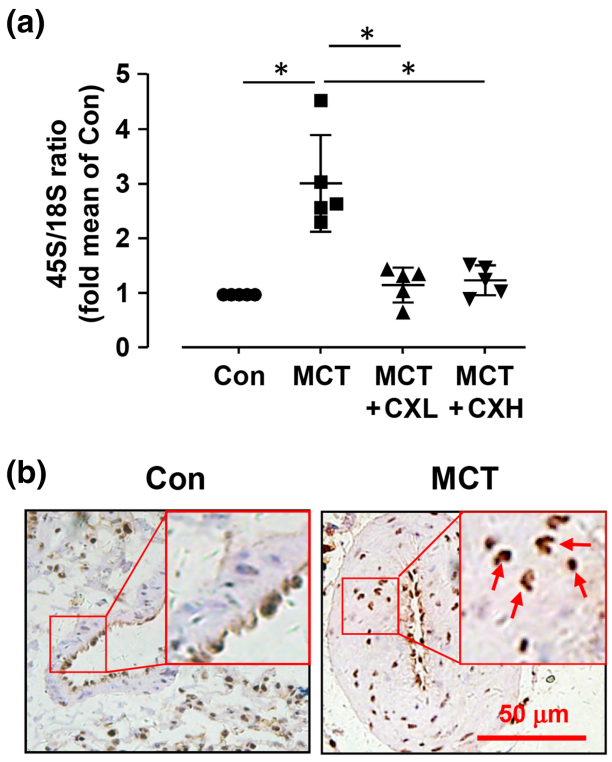

FIGURE 2 Altered rDNA transcriptional activity in the lungs with MCT-induced PAH (the prevention cohort). (a) Real-time PCR results showing changes in the ratio of 45S pre-rRNA to 18S mature rRNA in MCT-treated lungs and the effects of CX-5461. Con, normal control; MCT, disease models serving as vehicle control; CXL/CXH, PAH animals treated with low-dose (12.5 mg·kg^{-1})/high-dose (25 mg·kg^{-1}) CX-5461. (b) Immunohistochemistry staining showing an increased level of phospho-UBF (arrows) in the arterial wall in MCT-treated lungs. A relatively high level of phospho-UBF is also found in endothelial cells and some non-vascular cells in both groups. Data are mean ± SD. *P < .05, significantly different as indicated; Kruskal–Wallis test

result confirmed a significant beneficial effect of low-dose CX-5461 on survival (Figure S3).

3.5 | CX-5461 attenuates inflammatory cell infiltration in PAH lungs

We investigated whether CX-5461 therapy affected pulmonary inflammation using specimens from the MCT-prevention cohort. Similar to the results shown in Figure 3b, we demonstrated that most of the CD68$^+$ monocytes/macrophages, and CD8$^+$/CD4$^+$ T lymphocytes in PAH lungs were located in the vicinity of blood vessels (Figure 4). Treatment with low-dose CX-5461 significantly decreased the abundance of monocytes/macrophages and CD8$^+$ T cells, whereas there was no statistically significant change in CD4$^+$ T cells (Figure 4). We also confirmed that the level of **IL-6** was significantly lower in CX-5461-treated lungs (126.6 ± 10.1 pg·mg^{-1} in the low-dose CX-5461 group versus 154.5 ± 14.3 pg·mg^{-1} in the MCT group, Mann–Whitney test, n = 6).

3.6 | Effects of CX-5461 on PASMC cell cycle and p53 phosphorylation in vitro and in vivo

In human PASMCs in culture, CX-5461 at concentrations up to 2 μM did not induce obvious cytotoxic effects (exploratory data in Figure 5a). However, flow cytometry analysis revealed that CX-5461 treatment reduced the number of cells in S phase, indicating a cell cycle arrest at G1/S (Figure 5b). To confirm these results, we measured the expression of the S-phase marker PCNA by immunofluorescence. In a normal cell culture, CX-5461 treatment diminished the population of PCNA-positive cells (Figure 5c). In addition, the antiproliferative effect of CX-5461 was confirmed in vivo. As shown in Figure S4, the abundance of PCNA-positive cells in the medial layer of vessels in MCT-treated lungs was significantly reduced by CX-5461. It is known that inhibiting rDNA transcription in eukaryotes induces nucleolar stress, leading to stabilization and accumulation of p53 protein (Boulon et al., 2010). Similar to our findings in aortic smooth muscles (Ye et al., 2017), however, CX-5461 did not increase the total amount of p53 protein; instead it induced a robust increase in p53 phosphorylation (Figure 5d,e). Moreover, pretreatment with the selective p53 inhibitor pifithrin-α attenuated the inhibitory effect of CX-5461 on the cell cycle (see Figure 5b). In separate experiments, we confirmed that pifithrin-α alone had no significant effect on the cell cycle in normally proliferating cells without CX-5461, consistent with the very low level of p53 phosphorylation in untreated PASMCs (see Figure 5d).

To confirm the stimulatory effect of CX-5461 on p53 phosphorylation in vivo, we performed western blot experiments and demonstrated that CX-5461 significantly increased the level of phospho-p53 but not total p53 (data from MCT-prevention cohort) (Figure 5f). However, under the present experimental settings, we did not detect a significant change in the level of total p53 protein in PAH lungs. To further characterize the changes in p53 phosphorylation in blood vessels, we performed immunohistochemistry staining in MCT- and Su/H-treated lungs, and demonstrated that CX-5461 significantly increased the level of phospho-p53 in the medial layer, as compared to PAH models (Figures 5g and S5). These data reflected a trend of increased p53 function (phosphorylation) in PAH blood vessels by CX-5461, regardless of changes in the basal level of total p53 protein. These results suggested that the fundamental effect of CX-5461 on vascular remodelling in vivo was related to modulating p53 phosphorylation but not the level of total p53 (i.e., an increase in p-p53/total p53 ratio). To clarify whether CX-5461-induced p53 phosphorylation in vivo was associated with increased apoptosis of vascular cells, we performed TUNEL staining. In control, MCT and low-dose CX-5461 groups, apoptotic cells were not detected in the blood vessel wall, while a small number of apoptotic cells were similarly found in the latter two groups only in the non-vascular areas. In comparison, high-dose CX-5461 caused apoptosis of both vascular and non-vascular cells (Figure S6, data obtained from the MCT-prevention cohort). Moreover, we performed β-Gal staining assay to clarify whether CX-5461 promoted cell senescence and found that β-Gal-positive cells were absent from the vessel wall in all groups, while scattered

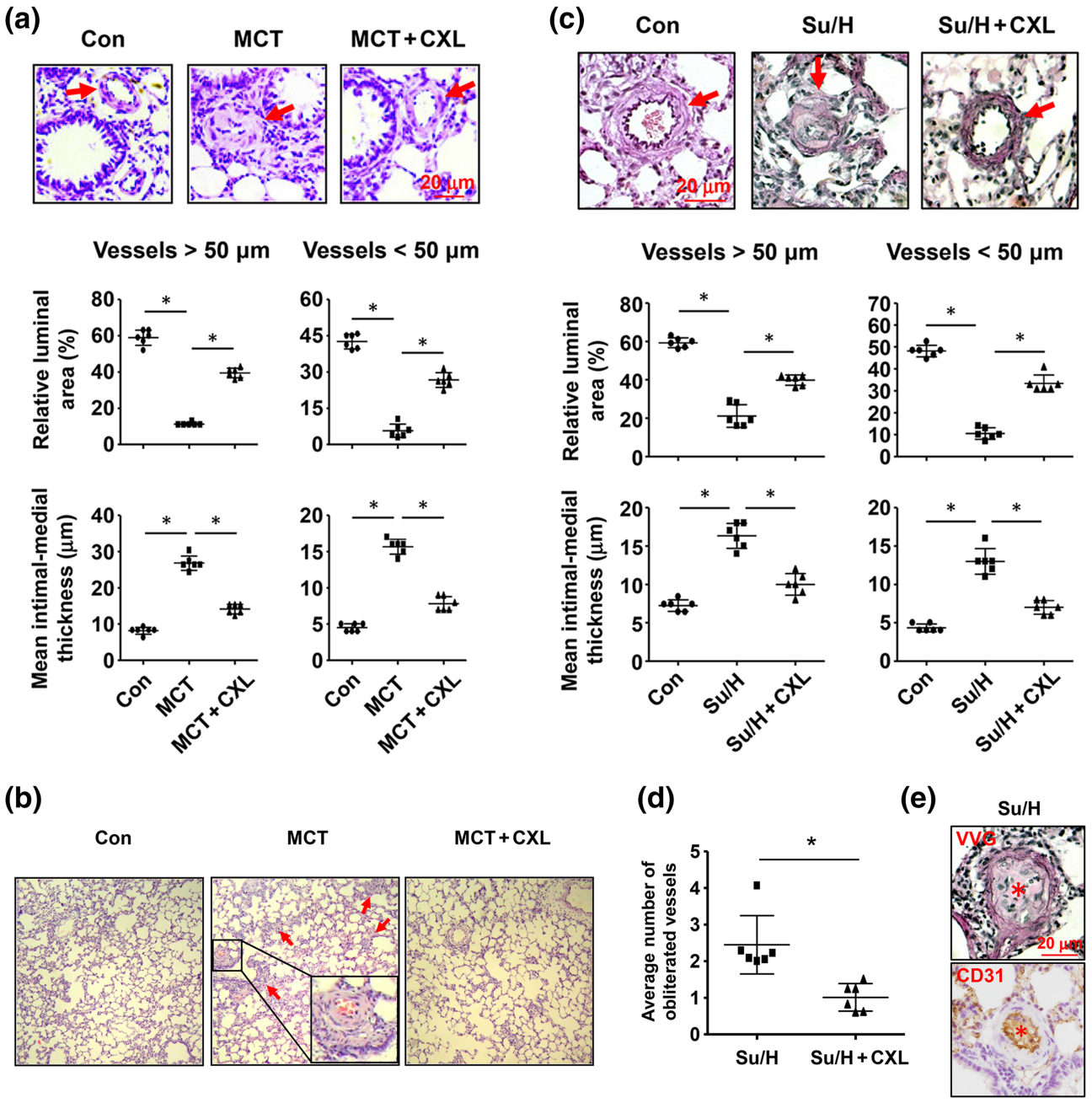

FIGURE 3 Low-dose (12.5 mg·kg^{-1}) CX-5461 (CXL) reverses established PAH. (a) H&E staining images and quantitative data showing that delayed treatment with CX-5461 partly reverses MCT-induced vascular remodelling (arrows). (b) H&E stained sections showing that CX-5461 reduces cellular infiltrations in MCT-treated lungs. Arrows indicate perivascular cell clumps. (c) Verhoeff–Van Gieson staining and quantitative data showing that CX-5461 partly reverses Su/H-induced vascular remodelling (arrows). (d) Effect of CX-5461 on the rate of vessel obliteration in Su/H-treated lungs (average number per 200X field). (e) Verhoeff–Van Gieson (VVG) and CD31 staining showing that the occlusive lesions induced by Su/H mainly contain CD31-positive neointimal tissues (asterisks). Data are mean ± SD. *P < .05, significantly different as indicated; one-way ANOVA or Mann–Whitney test as appropriate

β-Gal-positive cells could be detected in non-vascular areas only in the high-dose CX-5461 group (Figure S7). Taken together, these findings suggest that the anti-proliferative effect of low-dose CX-5461 in pulmonary vessels was mainly due to cell quiescence, but not senescence or apoptosis.

4 | DISCUSSION

In this study we demonstrated that oral administration of the selective Pol I inhibitor CX-5461 effectively inhibited the development of PAH and associated pulmonary arterial remodelling in two different rat

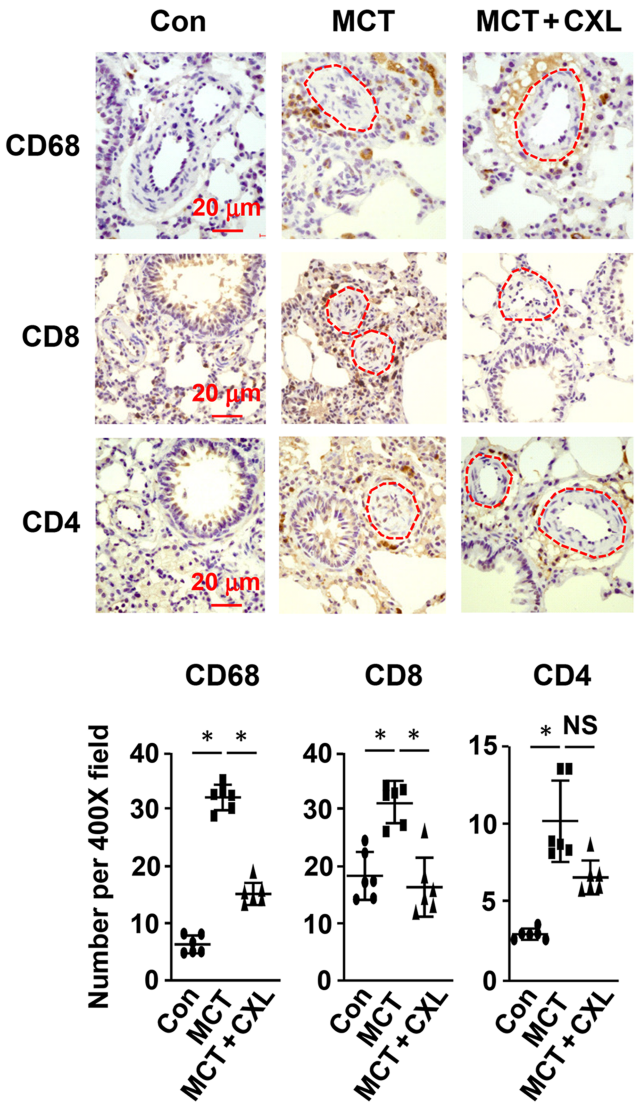

FIGURE 4 Immunohistochemistry images and corresponding quantitative data showing the effects of low-dose (12.5 mg·kg^{-1}) CX-5461 (CXL) on the abundance of CD68$^+$ monocytes/macrophages, CD8$^+$ T lymphocytes, and CD4$^+$ T lymphocytes in MCT-treated lungs (positive staining is in brown colour). Results are from the prevention cohort. Data are mean ± SD. *P < .05, significantly different as indicated; one-way ANOVA (for normally distributed data) or Kruskal–Wallis test (for non-normally distributed data t). NS, not significant. Dashed red lines indicate the position of blood vessels

models. Early treatment with CX-5461 prevented progress of the disease. Likewise, delayed treatment with the drug partly reversed the established PAH, together with beneficial effects on pulmonary vascular remodelling. Of note, the phase I dose-escalation study in patients with advanced haematological malignancies has shown that CX-5461 is a promising anti-tumor agent with favourable pharmacokinetics and safety profiles (Khot et al., 2019). Based on these data, we suggest that Pol I may represent a novel therapeutic target for limiting PAH and PAH-associated arterial remodelling. Currently, searching for new therapies for PAH remains a priority in both basic and clinical research, because clinically PAH is still associated with a poor prognosis despite significant advances in our understanding on the pathogenesis of this disease (Woodcock & Chan, 2019). Hence, selective Pol I inhibitors may give new hopes for PAH patients who are not responsive to available drug therapies. However, regression of developed RV hypertrophy in the reversal cohorts has not been observed in our study, although it can prevent RV hypertrophy in the early treatment group. We propose that a longer observational window may be required to elucidate the effect. In addition, our study was performed only in male animals, which was a weakness for translational potential since clinically PAH is more common in females.

Potent inhibitory effects of CX-5461 against pathological arterial remodelling have been observed in our previous studies in rat carotid arteries and aortae with angioplasty- or transplantation-induced injuries (Dai et al., 2018; Ye et al., 2017). Based on these data and those from the present study, we suggest that the beneficial effects of CX-5461 on PAH and associated vascular remodelling may involve different cellular mechanisms. Firstly, like its effects in aortic smooth muscle cells, CX-5461 directly elicits cell cycle blockade in PASMCs, although G1/S blockade predominates in the latter comparing with G2/M blockade in the former (Ye et al., 2017). It is clear that disruption of rDNA transcription triggers a distinct cellular stress response known as nucleolar stress, resulting in activation of the p53 pathway (Boulon et al., 2010; Yang et al., 2018). In contrast to the current paradigm which emphasizes stabilization and accumulation of p53 protein, following induction of nucleolar stress, we have repeatedly observed that CX-5461 had no major effects on total p53, but induced a robust response of p53 phosphorylation in a variety of cells (Dai et al., 2018; Ye et al., 2017), including human PASMCs, as used in the present study. Moreover, in the present study, we have confirmed that the cell cycle blockade in response to CX-5461 in human PASMCs is at least partly dependent on p53 as observed previously (Ye et al., 2017). Nonetheless, we could not exclude the possibility that CX-5461 might affect endothelial dysfunction associated with PAH, including reduced vasodilator functions, uncontrolled proliferation, aberrant paracrine activities and altered endothelial permeability.

Secondly, the beneficial effects of CX-5461 on PAH may be partly attributable to an anti-inflammatory property of the agent. We have reported that CX-5461 repressed vascular inflammation in transplanted aortic grafts (Dai et al., 2018). Here we confirmed that CX-5461 exerted potent anti-inflammatory effects in the lungs. Cells responsible for innate and adaptive immunity reactions are present in the lungs with PAH as revealed by both human and animal studies (Rabinovitch et al., 2014; Voelkel et al., 2016). In particular, CX-5461 treatment resulted in a ∼ 50% decrease in the number of macrophages in PAH lungs. There is evidence suggesting that the macrophage is crucially involved in the pathogenesis of PAH, as macrophage depletion retards disease progression (Jankov et al., 2001; Zaloudikova et al., 2016). Moreover, CX-5461 abolished the increase in CD8$^+$ T lymphocytes in the PAH group, but had no significant effect on CD4$^+$ T cells. Although infiltration of CD8$^+$ T cells is present in PAH lungs, the functional importance of these cells in the pathogenesis of PAH is currently inconclusive (Austin et al., 2010; Maston et al., 2017). Previously we showed that CX-5461 could

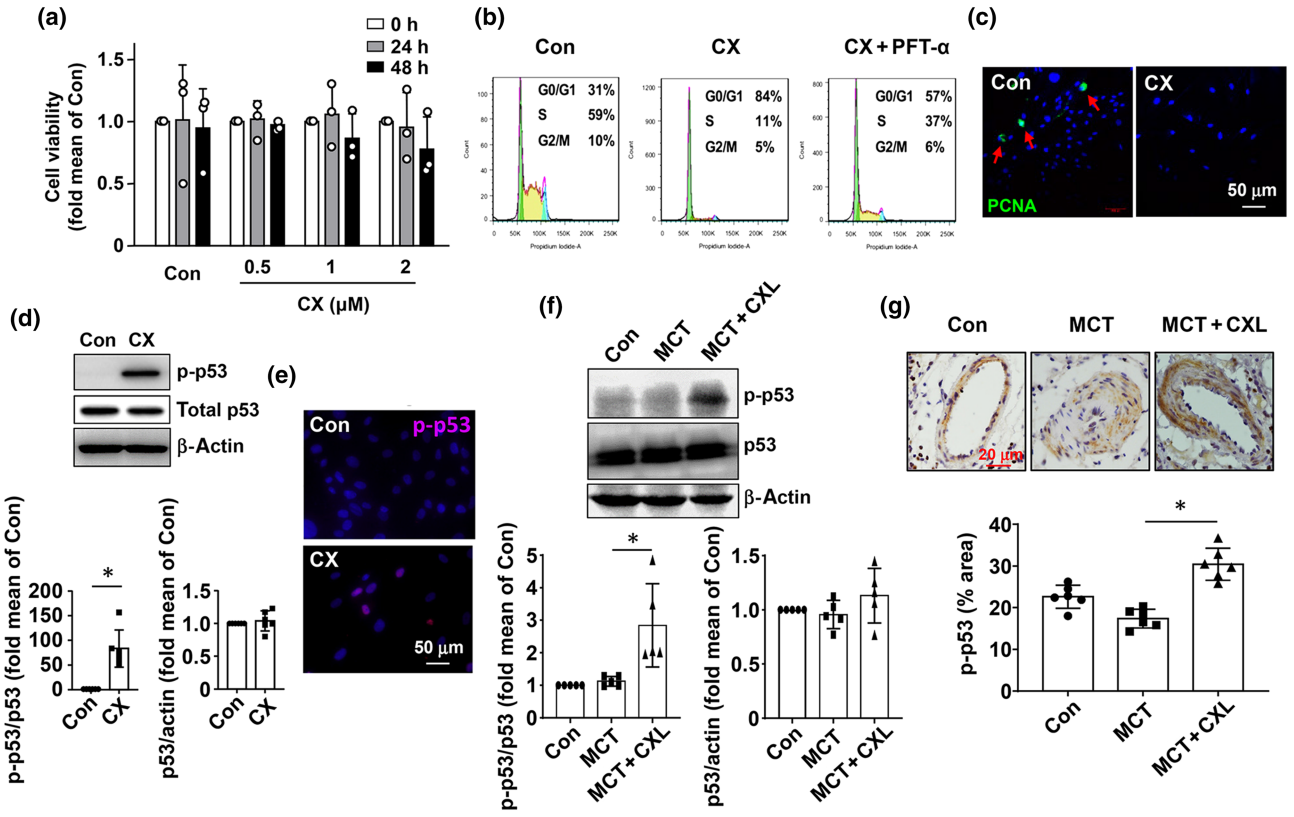

FIGURE 5 Effects of CX-5461 on PASMC cell cycle and p53 phosphorylation in vitro and in vivo. (a) Exploratory data showing that CX-5461 (0.5 to 2 μM) has no obvious effect on cell viability. (b) Representative flow cytometry results showing the effects of CX-5461 (2 μM for 24 h) on cell cycle in the presence and absence of the p53 inhibitor pifithrin-α (PFT-α, 2 μM). (c) Immunofluorescence images showing that CX-5461 (2 μM) diminishes the population of PCNA-positive cells in a normal cell culture. Nuclei are counterstained with DAPI (blue). (d) Representative western blots and quantitative densitometry data showing the effect of CX-5461 (2 μM) on the level of p53 phosphorylation. (e) Immunofluorescence images showing that CX-5461 (2 μM) increases the level of phospho-p53. Nuclei are counterstained with DAPI. (f) Representative western blots and densitometry data showing the in vivo effects of low-dose (12.5 $mg \cdot kg^{-1}$) CX-5461 (CXL) on levels of phospho-p53 and total p53 in MCT-treated lungs (prevention cohort). Con, normal control. (g) Immunohistochemistry and semi-quantitative immunoreactivity data showing the in vivo effect of low-dose CX-5461 on p53 phosphorylation (brown colour) in the arterial wall in PAH lungs (MCT-prevention cohort). Data are mean ± SD. *$P < .05$, significantly different as indicated; Kruskal–Wallis test or Mann–Whitney test as appropriate

inhibit macrophage functions including activation, migration, proliferation and differentiation/maturation (Dai et al., 2018). The lung tissue contains a variety of subpopulations of macrophages, which may play differential roles in homeostasis and/or inflammation (Duan & Croft, 2014). Further analysis of the specific effects of Pol I inhibition in these macrophage subpopulations is needed. Indeed, there is evidence suggesting that p53 has an anti-inflammatory role in macrophages (Belade et al., 2015; Mukhopadhyay et al., 2017; Zheng et al., 2005), which supports our findings of the anti-inflammatory effects of CX-5461.

Pol I inhibitors have been recognized to be a novel strategy to activate the p53 pathway (Ladds & Lain, 2019) and both genetic deletion and pharmacological inhibition of p53 aggravate the development of PAH in animal models (Jacquin et al., 2015; Mizuno et al., 2011). Further supporting our current results, Mouraret et al. (2013) have shown that nutlin-3, a small molecule that blocks the p53 degrading activity of the **ubiquitin ligase MDM2**, exhibits potent therapeutic effects against experimental pulmonary hypertension and suppresses pulmonary arterial remodelling. Similar to our observations, these authors demonstrated, in human PASMCs, that nutlin-3 induces cell growth arrest but not apoptosis, whereas whether nutlin-3 has any anti-inflammatory effect in the lungs has not been tested. Studies from other groups have also demonstrated that restoration of p53 functions may underlie the observed therapeutic effects by various interventions in experimental PAH (Abid et al., 2014; Jones et al., 2020). Nevertheless, it should be noted that smooth muscle cells are unlikely to be the only effector cell in vivo which mediate the beneficial effects of CX-5461 and p53 activation. For instance, a recent study has shown that smooth muscle-specific p53 overexpression is not sufficient to rescue hypoxia-induced PAH (Wakasugi et al., 2019), indicating that p53 functions in other type(s) of cells (e.g., inflammatory cells as suggested by our previous observations) (Dai et al., 2018) may also have important roles in modulating PAH.

A limitation of the present study is that our results cannot distinguish potential cell-specific contributions to the therapeutic effects of CX-5461. As such, there is a possibility that CX-5461 may indirectly inhibit PASMC proliferation by down-regulating the accumulation of inflammatory cells and/or production of pro-inflammatory cytokines. Based on the available data from different lines (Negi & Brown, 2015; Quin et al., 2016; Sanij et al., 2020; Ye et al., 2017), it is suggested that activation of the ATM/ATR-p53 axis has a pivotal role in mediating the pharmacological effects of CX-5461, although the perturbed rRNA synthesis and ribosome biogenesis may also make some contribution. However, we cannot either exclude the involvement of other signalling mechanisms in CX-5461-induced benefits, such as p53-independent effects of ATM/ATR kinases, and possible interactions with the **mTOR** pathway, which has a crucial role in the pathogenesis of PAH (Houssaini et al., 2013).

In summary, our study has identified a therapeutic effect of CX-5461 on experimental PAH and associated vascular remodelling, suggesting that pharmacological inhibition of Pol I may be a novel strategy to treat otherwise drug-resistant PAH.

ACKNOWLEDGEMENTS

This study was supported by grants from National Natural Science Foundation of China (81770469 for F.J. and 81500627 for X.C.), Key Research and Development Program of Shandong Province (2018GSF118011 for F.J., 2019GSF108052 for X.C., and 2019GSF108114 for X.X.), and Natural Science Foundation of Shandong Province (ZR2015HQ029 for X.C. and ZR2017BH047 for W.L.).

AUTHOR CONTRIBUTIONS

X.C., X.X., H.F., C.D., W.L., J.Z., X.G., and Q.Y. were involved in performing experiments and acquiring and analysing the experimental data; J.W. was involved in data analysis and data interpretation; X.C. and J.F. conceived the study, contributed to data interpretation, and drafted and revised the manuscript.

CONFLICT OF INTEREST

The authors declare no conflicts of interest.

DECLARATION OF TRANSPARENCY AND SCIENTIFIC RIGOUR

This Declaration acknowledges that this paper adheres to the principles for transparent reporting and scientific rigour of preclinical research as stated in the *BJP* guidelines for Natural Product Research, Design & Analysis, Immunoblotting and Immunochemistry, and Animal Experimentation, and as recommended by funding agencies, publishers, and other organizations engaged with supporting research.

DATA AVAILABILITY STATEMENT

The data that support the findings of this study are available from the corresponding author upon reasonable request.

ORCID

Fan Jiang https://orcid.org/0000-0001-9466-2192

REFERENCES

Abid, S., Houssaini, A., Mouraret, N., Marcos, E., Amsellem, V., Wan, F., Dubois-Randé, J. L., Derumeaux, G., Boczkowski, J., Motterlini, R., & Adnot, S. (2014). P21-dependent protective effects of a carbon monoxide-releasing molecule-3 in pulmonary hypertension. *Arteriosclerosis, Thrombosis, and Vascular Biology*, *34*(2), 304–312. https://doi.org/10.1161/ATVBAHA.113.302302

Alexander, S. P. H., Fabbro, D., Kelly, E., Mathie, A., Peters, J. A., Veale, E. L., Armstrong, J. F., Faccenda, E., Harding, S. D., Pawson, A. J., & Sharman, J. L. (2019). The Concise Guide to PHARMACOLOGY 2019/20: Enzymes. *British Journal of Pharmacology*, *176*, S297–S396. https://doi.org/10.1111/bph.14752

Alexander, S. P. H., Roberts, R. E., Broughton, B. R. S., Sobey, C. G., George, C. H., Stanford, S. C., Cirino, G., Docherty, J. R., Giembycz, M. A., Hoyer, D., & Insel, P. A. (2018). Goals and practicalities of immunoblotting and immunohistochemistry: A guide for submission to the *British Journal of Pharmacology*. *British Journal of Pharmacology*, *175*(3), 407–411.

Amsellem, V., Abid, S., Poupel, L., Parpaleix, A., Rodero, M., Gary-Bobo, G., Latiri, M., Dubois-Rande, J. L., Lipskaia, L., Combadiere, C., & Adnot, S. (2017). Roles for the CX3CL1/CX3CR1 and CCL2/CCR2 chemokine systems in hypoxic pulmonary hypertension. *American Journal of Respiratory Cell and Molecular Biology*, *56*(5), 597–608. https://doi.org/10.1165/rcmb.2016-0201OC

Austin, E. D., Rock, M. T., Mosse, C. A., Vnencak-Jones, C. L., Yoder, S. M., Robbins, I. M., Loyd, J. E., & Meyrick, B. O. (2010). T lymphocyte subset abnormalities in the blood and lung in pulmonary arterial hypertension. *Respiratory Medicine*, *104*(3), 454–462. https://doi.org/10.1016/j.rmed.2009.10.004

Belade, E., Chrusciel, S., Armand, L., Simon-Deckers, A., Bussy, C., Caramelle, P., Gagliolo, J. M., Boyer, L., Lanone, S., Pairon, J. C., & Kermanizadeh, A. (2015). The role of p53 in lung macrophages following exposure to a panel of manufactured nanomaterials. *Archives of Toxicology*, *89*(9), 1543–1556. https://doi.org/10.1007/s00204-014-1324-5

Boulon, S., Westman, B. J., Hutten, S., Boisvert, F. M., & Lamond, A. I. (2010). The nucleolus under stress. *Molecular Cell*, *40*(2), 216–227. https://doi.org/10.1016/j.molcel.2010.09.024

Bywater, M. J., Pearson, R. B., McArthur, G. A., & Hannan, R. D. (2013). Dysregulation of the basal RNA polymerase transcription apparatus in cancer. *Nature Reviews Cancer*, *13*(5), 299–314. https://doi.org/10.1038/nrc3496

Bywater, M. J., Poortinga, G., Sanij, E., Hein, N., Peck, A., Cullinane, C., Wall, M., Cluse, L., Drygin, D., Anderes, K., & Huser, N. (2012). Inhibition of RNA polymerase I as a therapeutic strategy to promote cancer-specific activation of p53. *Cancer Cell*, *22*(1), 51–65. https://doi.org/10.1016/j.ccr.2012.05.019

Cornelison, R., Dobbin, Z. C., Katre, A. A., Jeong, D. H., Zhang, Y., Chen, D., Petrova, Y., Llaneza, D. C., Steg, A. D., Parsons, L., & Schneider, D. A. (2017). Targeting RNA-polymerase I in both chemosensitive and chemoresistant populations in epithelial ovarian cancer. *Clinical Cancer Research*, *23*(21), 6529–6540. https://doi.org/10.1158/1078-0432.CCR-17-0282

Curtis, M. J., Alexander, S., Cirino, G., Docherty, J. R., George, C. H., Giembycz, M. A., Hoyer, D., Insel, P. A., Izzo, A. A., Ji, Y., & MacEwan, D. J. (2018). Experimental design and analysis and their reporting II: Updated and simplified guidance for authors and peer reviewers. *British Journal of Pharmacology*, *175*(7), 987–993. https://doi.org/10.1111/bph.14153

Dai, C., Sun, M., Wang, F., Zhu, J., Wei, Y., Guo, X., Ma, S., Dong, B., Wang, G., Jiang, F., & Wang, J. (2018). The selective RNA polymerase I inhibitor CX-5461 mitigates neointimal remodeling in a modified model of rat aortic transplantation. *Transplantation*, *102*(10), 1674–1683.

Dean, A., Nilsen, M., Loughlin, L., Salt, I. P., & MacLean, M. R. (2016). Metformin reverses development of pulmonary hypertension via

aromatase inhibition. *Hypertension*, *68*(2), 446–454. https://doi.org/10.1161/HYPERTENSIONAHA.116.07353

Drygin, D., Lin, A., Bliesath, J., Ho, C. B., O'Brien, S. E., Proffitt, C., Omori, M., Haddach, M., Schwaebe, M. K., Siddiqui-Jain, A., & Streiner, N. (2011). Targeting RNA polymerase I with an oral small molecule CX-5461 inhibits ribosomal RNA synthesis and solid tumor growth. *Cancer Research*, *71*(4), 1418–1430. https://doi.org/10.1158/0008-5472.CAN-10-1728

Duan, W., & Croft, M. (2014). Control of regulatory T cells and airway tolerance by lung macrophages and dendritic cells. *Annals of the American Thoracic Society*, *11*(Suppl 5), S306–S313. https://doi.org/10.1513/AnnalsATS.201401-028AW

Farhat, M. Y., Chen, M. F., Bhatti, T., Iqbal, A., Cathapermal, S., & Ramwell, P. W. (1993). Protection by oestradiol against the development of cardiovascular changes associated with monocrotaline pulmonary hypertension in rats. *British Journal of Pharmacology*, *110*(2), 719–723. https://doi.org/10.1111/j.1476-5381.1993.tb13871.x

Frumkin, L. R. (2012). The pharmacological treatment of pulmonary arterial hypertension. *Pharmacological Reviews*, *64*(3), 583–620. https://doi.org/10.1124/pr.111.005587

Handoko, M. L., de Man, F. S., Happe, C. M., Schalij, I., Musters, R. J., Westerhof, N., Postmus, P. E., Paulus, W. J., & Van Der Laarse, W. J. (2009). Opposite effects of training in rats with stable and progressive pulmonary hypertension. *Circulation*, *120*(1), 42–49. https://doi.org/10.1161/CIRCULATIONAHA.108.829713

Happe, C. M., de Raaf, M. A., Rol, N., Schalij, I., Vonk-Noordegraaf, A., Westerhof, N., Voelkel, N. F., de Man, F. S., & Bogaard, H. J. (2016). Pneumonectomy combined with SU5416 induces severe pulmonary hypertension in rats. *American Journal of Physiology. Lung Cellular and Molecular Physiology*, *310*(11), L1088–L1097.

Hoidal, J. R., Brar, S. S., Sturrock, A. B., Sanders, K. A., Dinger, B., Fidone, S., & Kennedy, T. P. (2003). The role of endogenous NADPH oxidases in airway and pulmonary vascular smooth muscle function. *Antioxidants & Redox Signaling*, *5*(6), 751–758. https://doi.org/10.1089/152308603770380052

Houssaini, A., Abid, S., Mouraret, N., Wan, F., Rideau, D., Saker, M., Marcos, E., Tissot, C. M., Dubois-Randé, J. L., Amsellem, V., & Adnot, S. (2013). Rapamycin reverses pulmonary artery smooth muscle cell proliferation in pulmonary hypertension. *American Journal of Respiratory Cell and Molecular Biology*, *48*(5), 568–577. https://doi.org/10.1165/rcmb.2012-0429OC

Humbert, M., Morrell, N. W., Archer, S. L., Stenmark, K. R., MacLean, M. R., Lang, I. M., Christman, B. W., Weir, E. K., Eickelberg, O., Voelkel, N. F., & Rabinovitch, M. (2004). Cellular and molecular pathobiology of pulmonary arterial hypertension. *Journal of the American College of Cardiology*, *43*(12 Suppl S), 13S–24S.

Hurst, L. A., Dunmore, B. J., Long, L., Crosby, A., Al-Lamki, R., Deighton, J., Southwood, M., Yang, X., Nikolic, M. Z., Herrera, B., & Inman, G. J. (2017). TNFα drives pulmonary arterial hypertension by suppressing the BMP type-II receptor and altering NOTCH signalling. *Nature Communications*, *8*, 14079. https://doi.org/10.1038/ncomms14079

Jacquin, S., Rincheval, V., Mignotte, B., Richard, S., Humbert, M., Mercier, O., Londoño-Vallejo, A., Fadel, E., & Eddahibi, S. (2015). Inactivation of p53 is sufficient to induce development of pulmonary hypertension in rats. *PLoS One*, *10*(6), e0131940. https://doi.org/10.1371/journal.pone.0131940

Janakidevi, K., Fisher, M. A., Del Vecchio, P. J., Tiruppathi, C., Figge, J., & Malik, A. B. (1992). Endothelin-1 stimulates DNA synthesis and proliferation of pulmonary artery smooth muscle cells. *American Journal of Physiology*, *263*(6 Pt 1), C1295–C1301. https://doi.org/10.1152/ajpcell.1992.263.6.C1295

Jankov, R. P., Luo, X., Belcastro, R., Copland, I., Frndova, H., Lye, S. J., Hoidal, J. R., Post, M., & Tanswell, A. K. (2001). Gadolinium chloride inhibits pulmonary macrophage influx and prevents O_2-induced pulmonary hypertension in the neonatal rat. *Pediatric Research*, *50*(2), 172–183. https://doi.org/10.1203/00006450-200108000-00003

Jones, C., Bisserier, M., Bueno-Beti, C., Bonnet, G., Neves-Zaph, S., Lee, S. Y., Milara, J., Dorfmüller, P., Humbert, M., Leopold, J. A., & Hadri, L. (2020). A novel secreted-cAMP pathway inhibits pulmonary hypertension via a feed-forward mechanism. *Cardiovascular Research*, *116*(8), 1500–1513. https://doi.org/10.1093/cvr/cvz244

Jones, G. T., Jiang, F., McCormick, S. P., & Dusting, G. J. (2005). Elastic lamina defects are an early feature of aortic lesions in the apolipoprotein E knockout mouse. *Journal of Vascular Research*, *42*(3), 237–246. https://doi.org/10.1159/000085553

Khot, A., Brajanovski, N., Cameron, D. P., Hein, N., Maclachlan, K. H., Sanij, E., Lim, J., Soong, J., Link, E., Blombery, P., & Thompson, E. R. (2019). First-in-human RNA polymerase I transcription inhibitor CX-5461 in patients with advanced hematologic cancers: Results of a phase I dose-escalation study. *Cancer Discovery*, *9*(8), 1036–1049. https://doi.org/10.1158/2159-8290.CD-18-1455

Ladds, M., & Lain, S. (2019). Small molecule activators of the p53 response. *Journal of Molecular Cell Biology*, *11*(3), 245–254. https://doi.org/10.1093/jmcb/mjz006

Lee, H. C., Wang, H., Baladandayuthapani, V., Lin, H., He, J., Jones, R. J., Kuiatse, I., Gu, D., Wang, Z., Ma, W., & Lim, J. (2017). RNA polymerase I inhibition with CX-5461 as a novel therapeutic strategy to target MYC in multiple myeloma. *British Journal of Haematology*, *177*(1), 80–94. https://doi.org/10.1111/bjh.14525

Lee, S. H., & Rubin, L. J. (2005). Current treatment strategies for pulmonary arterial hypertension. *Journal of Internal Medicine*, *258*(3), 199–215. https://doi.org/10.1111/j.1365-2796.2005.01542.x

Lilley, E., Stanford, S. C., Kendall, D. E., Alexander, S. P.H., Cirino, G., Docherty, J. R., George, C. H., Insel, P. A., Izzo, A. A., Ji, Y., Panettieri, R. A., Sobey, C. G., Stefanska, B., Stephens, G., Teixeira, M., & Ahluwalia, A. (2020). ARRIVE 2.0 and the British Journal of Pharmacology: Updated guidance for 2020. *British Journal of Pharmacology*, *177*(16), 3611–3616. https://doi.org/10.1111/bph.15178

Liu, H., Ge, X. Y., Huang, N., Liu, T., Yao, M. Z., Zhang, Z., Qian, Z. X., & Hu, C. P. (2019). Up-regulation of cullin7 promotes proliferation and migration of pulmonary artery smooth muscle cells in hypoxia-induced pulmonary hypertension. *European Journal of Pharmacology*, *864*, 172698. https://doi.org/10.1016/j.ejphar.2019.172698

Livak, K. J., & Schmittgen, T. D. (2001). Analysis of relative gene expression data using real-time quantitative PCR and the $2^{-\Delta\Delta C}{}_T$ method. *Methods*, *25*(4), 402–408. https://doi.org/10.1006/meth.2001.1262

Maston, L. D., Jones, D. T., Giermakowska, W., Howard, T. A., Cannon, J. L., Wang, W., Wei, Y., Xuan, W., Resta, T. C., & Bosc, L. V. (2017). Central role of T helper 17 cells in chronic hypoxia-induced pulmonary hypertension. *American Journal of Physiology. Lung Cellular and Molecular Physiology*, *312*(5), L609–L624.

Mizuno, S., Bogaard, H. J., Kraskauskas, D., Alhussaini, A., Gomez-Arroyo, J., Voelkel, N. F., & Ishizaki, T. (2011). p53 gene deficiency promotes hypoxia-induced pulmonary hypertension and vascular remodeling in mice. *American Journal of Physiology. Lung Cellular and Molecular Physiology*, *300*(5), L753–L761.

Morrell, N. W. (2006). Pulmonary hypertension due to BMPR2 mutation: A new paradigm for tissue remodeling? *Proceedings of the American Thoracic Society*, *3*(8), 680–686. https://doi.org/10.1513/pats.200605-118SF

Mouraret, N., Marcos, E., Abid, S., Gary-Bobo, G., Saker, M., Houssaini, A., Dubois-Rande, J. L., Boyer, L., Boczkowski, J., Derumeaux, G., & Amsellem, V. (2013). Activation of lung p53 by Nutlin-3a prevents and reverses experimental pulmonary hypertension. *Circulation*, *127*(16), 1664–1676. https://doi.org/10.1161/CIRCULATIONAHA.113.002434

Mukhopadhyay, S., Antalis, T. M., Nguyen, K. P., Hoofnagle, M. H., & Sarkar, R. (2017). Myeloid p53 regulates macrophage polarization and

venous thrombus resolution by inflammatory vascular remodeling in mice. *Blood*, *129*(24), 3245–3255. https://doi.org/10.1182/blood-2016-07-727180

Negi, S. S., & Brown, P. (2015). rRNA synthesis inhibitor, CX-5461, activates ATM/ATR pathway in acute lymphoblastic leukemia, arrests cells in G2 phase and induces apoptosis. *Oncotarget*, *6*(20), 18094–18104. https://doi.org/10.18632/oncotarget.4093

Nickel, N. P., Spiekerkoetter, E., Gu, M., Li, C. G., Li, H., Kaschwich, M., Diebold, I., Hennigs, J. K., Kim, K. Y., Miyagawa, K., & Wang, L. (2015). Elafin reverses pulmonary hypertension via caveolin-1-dependent bone morphogenetic protein signaling. *American Journal of Respiratory and Critical Care Medicine*, *191*(11), 1273–1286. https://doi.org/10.1164/rccm.201412-2291OC

Oka, M., Homma, N., Taraseviciene-Stewart, L., Morris, K. G., Kraskauskas, D., Burns, N., Voelkel, N. F., & McMurtry, I. F. (2007). Rho kinase-mediated vasoconstriction is important in severe occlusive pulmonary arterial hypertension in rats. *Circulation Research*, *100*(6), 923–929. https://doi.org/10.1161/01.RES.0000261658.12024.18

Paddenberg, R., Stieger, P., von Lilien, A. L., Faulhammer, P., Goldenberg, A., Tillmanns, H. H., Kummer, W., & Braun-Dullaeus, R. C. (2007). Rapamycin attenuates hypoxia-induced pulmonary vascular remodeling and right ventricular hypertrophy in mice. *Respiratory Research*, *8*(1), 15. https://doi.org/10.1186/1465-9921-8-15

Percie du Sert, N., Hurst, V., Ahluwalia, A., Alam, S., Avey, M. T., Baker, M., Browne, W. J., Clark, A., Cuthill, I. C., Dirnagl, U., & Emerson, M. (2020). The ARRIVE guidelines 2.0: Updated guidelines for reporting animal research. *PLoS Biology*, *18*(7), e3000410. https://doi.org/10.1371/journal.pbio.3000410

Preston, I. R., Hill, N. S., Warburton, R. R., & Fanburg, B. L. (2006). Role of 12-lipoxygenase in hypoxia-induced rat pulmonary artery smooth muscle cell proliferation. *American Journal of Physiology. Lung Cellular and Molecular Physiology*, *290*(2), L367–L374.

Price, L. C., Wort, S. J., Perros, F., Dorfmuller, P., Huertas, A., Montani, D., Cohen-Kaminsky, S., & Humbert, M. (2012). Inflammation in pulmonary arterial hypertension. *Chest*, *141*(1), 210–221. https://doi.org/10.1378/chest.11-0793

Quin, J., Chan, K. T., Devlin, J. R., Cameron, D. P., Diesch, J., Cullinane, C., Ahern, J., Khot, A., Hein, N., George, A. J., & Hannan, R. D. (2016). Inhibition of RNA polymerase I transcription initiation by CX-5461 activates non-canonical ATM/ATR signaling. *Oncotarget*, *7*(31), 49800–49818. https://doi.org/10.18632/oncotarget.10452

Rabinovitch, M., Guignabert, C., Humbert, M., & Nicolls, M. R. (2014). Inflammation and immunity in the pathogenesis of pulmonary arterial hypertension. *Circulation Research*, *115*(1), 165–175. https://doi.org/10.1161/CIRCRESAHA.113.301141

Sanij, E., Hannan, K. M., Xuan, J., Yan, S., Ahern, J. E., Trigos, A. S., Brajanovski, N., Son, J., Chan, K. T., Kondrashova, O., & Lieschke, E. (2020). CX-5461 activates the DNA damage response and demonstrates therapeutic efficacy in high-grade serous ovarian cancer. *Nature Communications*, *11*(1), 2641. https://doi.org/10.1038/s41467-020-16393-4

Savai, R., Pullamsetti, S. S., Kolbe, J., Bieniek, E., Voswinckel, R., Fink, L., Scheed, A., Ritter, C., Dahal, B. K., Vater, A., & Klussmann, S. (2012). Immune and inflammatory cell involvement in the pathology of idiopathic pulmonary arterial hypertension. *American Journal of Respiratory and Critical Care Medicine*, *186*(9), 897–908. https://doi.org/10.1164/rccm.201202-0335OC

Shimoda, L. A., & Laurie, S. S. (2013). Vascular remodeling in pulmonary hypertension. *Journal of Molecular Medicine (Berlin)*, *91*(3), 297–309. https://doi.org/10.1007/s00109-013-0998-0

Sneddon, L. U., Halsey, L. G., & Bury, N. R. (2017). Considering aspects of the 3Rs principles within experimental animal biology. *Journal of Experimental Biology*, *220*(Pt 17), 3007–3016. https://doi.org/10.1242/jeb.147058

Spiekerkoetter, E., Tian, X., Cai, J., Hopper, R. K., Sudheendra, D., Li, C. G., El-Bizri, N., Sawada, H., Haghighat, R., Chan, R., & Haghighat, L. (2013). FK506 activates BMPR2, rescues endothelial dysfunction, and reverses pulmonary hypertension. *Journal of Clinical Investigation*, *123*(8), 3600–3613. https://doi.org/10.1172/JCI65592

Thompson, A. A., & Lawrie, A. (2017). Targeting vascular remodeling to treat pulmonary arterial hypertension. *Trends in Molecular Medicine*, *23*(1), 31–45. https://doi.org/10.1016/j.molmed.2016.11.005

Tuder, R. M., Marecki, J. C., Richter, A., Fijalkowska, I., & Flores, S. (2007). Pathology of pulmonary hypertension. *Clinics in Chest Medicine*, *28*(1), 23–42. https://doi.org/10.1016/j.ccm.2006.11.010

Voelkel, N. F., Tamosiuniene, R., & Nicolls, M. R. (2016). Challenges and opportunities in treating inflammation associated with pulmonary hypertension. *Expert Review of Cardiovascular Therapy*, *14*(8), 939–951. https://doi.org/10.1080/14779072.2016.1180976

Wakasugi, T., Shimizu, I., Yoshida, Y., Hayashi, Y., Ikegami, R., Suda, M., Katsuumi, G., Nakao, M., Hoyano, M., Kashimura, T., & Nakamura, K. (2019). Role of smooth muscle cell p53 in pulmonary arterial hypertension. *PLoS One*, *14*(2), e0212889. https://doi.org/10.1371/journal.pone.0212889

Wang, Z., Yang, K., Zheng, Q., Zhang, C., Tang, H., Babicheva, A., Jiang, Q., Li, M., Chen, Y., Carr, S. G., & Wu, K. (2019). Divergent changes of p53 in pulmonary arterial endothelial and smooth muscle cells involved in the development of pulmonary hypertension. *American Journal of Physiology. Lung Cellular and Molecular Physiology*, *316*(1), L216–L228.

White, R. J. (2005). RNA polymerases I and III, growth control and cancer. *Nature Reviews Molecular Cell Biology*, *6*(1), 69–78. https://doi.org/10.1038/nrm1551

Woodcock, C. C., & Chan, S. Y. (2019). The search for disease-modifying therapies in pulmonary hypertension. *Journal of Cardiovascular Pharmacology and Therapeutics*, *24*(4), 334–354. https://doi.org/10.1177/1074248419829172

Wynants, M., Quarck, R., Ronisz, A., Alfaro-Moreno, E., Van Raemdonck, D., Meyns, B., & Delcroix, M. (2012). Effects of C-reactive protein on human pulmonary vascular cells in chronic thromboembolic pulmonary hypertension. *European Respiratory Journal*, *40*(4), 886–894. https://doi.org/10.1183/09031936.00197511

Xu, D., Guo, H., Xu, X., Lu, Z., Fassett, J., Hu, X., Xu, Y., Tang, Q., Hu, D., Somani, A., & Geurts, A. M. (2011). Exacerbated pulmonary arterial hypertension and right ventricular hypertrophy in animals with loss of function of extracellular superoxide dismutase. *Hypertension*, *58*(2), 303–309. https://doi.org/10.1161/HYPERTENSIONAHA.110.166819

Yang, K., Yang, J., & Yi, J. (2018). Nucleolar stress: Hallmarks, sensing mechanism and diseases. *Cell Stress*, *2*, 125–140.

Ye, Q., Pang, S., Zhang, W., Guo, X., Wang, J., Zhang, Y., Liu, Y., Wu, X., & Jiang, F. (2017). Therapeutic targeting of RNA polymerase I with the small-molecule CX-5461 for prevention of arterial injury-induced neointimal hyperplasia. *Arteriosclerosis, Thrombosis, and Vascular Biology*, *37*(3), 476–484. https://doi.org/10.1161/ATVBAHA.116.308401

Zabini, D., Crnkovic, S., Xu, H., Tscherner, M., Ghanim, B., Klepetko, W., Olschewski, A., Kwapiszewska, G., & Marsh, L. M. (2015). High-mobility group box-1 induces vascular remodelling processes via c-Jun activation. *Journal of Cellular and Molecular Medicine*, *19*(5), 1151–1161. https://doi.org/10.1111/jcmm.12519

Zaloudikova, M., Vytasek, R., Vajnerova, O., Hnilickova, O., Vizek, M., Hampl, V., & Herget, J. (2016). Depletion of alveolar macrophages attenuates hypoxic pulmonary hypertension but not hypoxia-induced increase in serum concentration of MCP-1. *Physiological Research*, *65*(5), 763–768. https://doi.org/10.33549/physiolres.933187

Zheng, S. J., Lamhamedi-Cherradi, S. E., Wang, P., Xu, L., & Chen, Y. H. (2005). Tumor suppressor p53 inhibits autoimmune inflammation and

macrophage function. *Diabetes*, *54*(5), 1423–1428. https://doi.org/10.2337/diabetes.54.5.1423

SUPPORTING INFORMATION

Additional supporting information may be found online in the Supporting Information section at the end of this article.

How to cite this article: Xu X, Feng H, Dai C, et al. Therapeutic efficacy of the novel selective RNA polymerase I inhibitor CX-5461 on pulmonary arterial hypertension and associated vascular remodelling. *Br J Pharmacol*. 2021;178:1605–1619. https://doi.org/10.1111/bph.15385